Journal Pre-proof

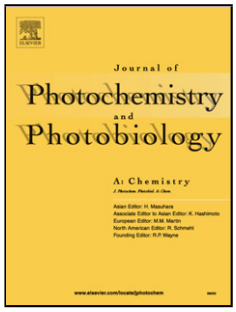

Stabilization of p-GaAs electrode surfaces in organic solvent by bi-phenyl rings for spin dependent electron transfer studies<!–<ForCover>Tamski M, Ansermet JP, Roussel C, Stabilization of p-GaAs electrode surfaces in organic solvent by bi-phenyl rings for spin dependent electron transfer studies, *Journal of Photochemistry and amp; Photobiology, A: Chemistry*, doi: 10.1016/j.jphotochem.2020.112853</ForCover>–>

M. Tamski, J.P. Ansermet, C. Roussel

PII: S1010-6030(20)30651-1

DOI: https://doi.org/10.1016/j.jphotochem.2020.112853

Reference: JPC 112853

To appear in: *Journal of Photochemistry & Photobiology, A: Chemistry*

Received Date: 10 April 2020

Revised Date: 9 August 2020

Accepted Date: 14 August 2020

Please cite this article as: { doi: https://doi.org/

This is a PDF file of an article that has undergone enhancements after acceptance, such as the addition of a cover page and metadata, and formatting for readability, but it is not yet the definitive version of record. This version will undergo additional copyediting, typesetting and review before it is published in its final form, but we are providing this version to give early visibility of the article. Please note that, during the production process, errors may be discovered which could affect the content, and all legal disclaimers that apply to the journal pertain.

© 2020 Published by Elsevier.

Journal Pre-proof

Stabilization of p-GaAs electrode surfaces in organic solvent by bi-phenyl rings for spin dependent electron transfer studies

M. Tamski[a], J.-P. Ansermet[a] and C. Roussel[a,b]

[a]Institute of Physics, Ecole Polytechnique Fédérale de Lausanne (EPFL), 1015 Lausanne, Switzerland
[b]SCGC, Ecole Polytechnique Fédérale de Lausanne (EPFL), 1015 Lausanne, Switzerland

Jean-Philippe Ansermet, e-mail: jean-philippe.ansermet@epfl.ch

ORCID number: 0000-0002-1307-4864

Christophe Roussel, e-mail: christophe.roussel@epfl.ch, ORCID number: 0000-0001-9631-1468

Corresponding Author

*Mika Tamski, e-mail: mika.tamski@epfl.ch, ORCID number: 0000-0002-1707-7800

Graphical Abstract

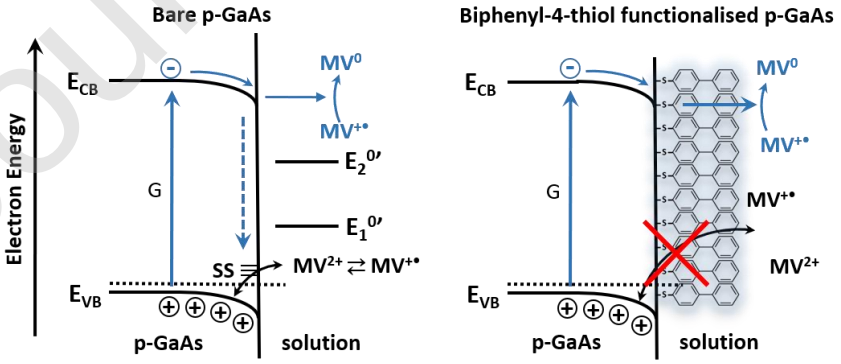

Journal Pre-proof

Highlights

- p-GaAs photocathodes were functionalised with biphenol-4-thiol monolayers
- Functionalisation did not hinder the electron transfer rate in acetonitrile
- Energy diagrams were obtained to explain the electron transfer with and without functionalisation.
- The functionalised p-GaAs electrode was stabilised against surface state mediated processes

Abstract

Biphenyl-4-thiol (B4t) functionalised p-GaAs photocathodes were compared to non-functionalised p-GaAs ones in the presence of methyl viologen cation radical ($MV^{+\bullet}$) as a redox mediator. Cyclic voltammetry (CV) and electrochemical impedance spectroscopy (EIS) studies revealed that at bare p-GaAs photocathodes the radical interacts strongly with the electrode surface, displaying unwanted surface states (SS) mediated electron transfer (ET) even in the dark. Functionalising the electrode with B4t passivated the interface against this unwanted process, while ensuring that the conduction band (CB) electrons still facilitated faradaic reduction of $MV^{+\bullet}$ to MV^{0} with unhindered efficiency.

Keywords: p-GaAs, functionalisation, methylviologen, photocathode, Electrochemical Impedance Spectroscopy, biphenyl-4-thiol

1. Introduction

GaAs semiconductors attract considerable interest in many fields, particularly in photovoltaics and in conversion of solar to chemical energy.[1–7] Previous research has often highlighted the chemical instability of GaAs to be one of the main problems in its adoption as an electrode material in electrochemistry.[8–13] This issue is especially prevalent in the case of p-GaAs, where the majority charge carriers are holes. p-doped GaAs (p-GaAs) is also reported as an interesting material for spin dependent electrochemical studies,[14,15] our field of interest.

In our approach, a spin-oriented electron transfer (ET) is induced from a p-GaAs semiconductor to a radical redox mediator polarized in solution by a magnetic field. The spin orientation of the electrons of the semiconductor occurs during the promotion of valence band (VB) electrons to the empty conducting band (CB) through optical pumping using a polarized light under weak illumination,[16] i.e. conditions for which a spin-dependent ET kinetics have been already observed.[14,15] In such a process, the spin polarization of the CB electrons must be conserved during the ET, so any process involving spin relaxation prior to the ET must be avoided.

The question of the ET pathways at semiconductor/solution interface has been discussed extensively in the literature.[17–20] We have recently characterised the photocathodic behaviour of p-GaAs towards 1,4-benzoquinone (BQ) and Tris(2,2'-bipyridine)ruthenium(II) hexafluorophosphate ($Ru(bpy)_3^{2+}$) in acetonitrile under weak illumination conditions.[21] Our study has highlighted that in the presence of BQ the ET originates from the CB, whereas in the presence of $Ru(bpy)_3^{2+}$, the surface states (SS) of the semiconductor play an important role in the ET process.

We also recently reported on the spin dependent ET at chiral and non-chiral electrodes using methyl viologen cation radical ($MV^{+\bullet}$) as redox mediator to explore chirality-induced spin selectivity (CISS).[16]

Journal Pre-proof

In this work, the chiral electrodes were made of an α-helical polypeptide layer terminated with Ag nanoparticles deposited on an Au-covered GaN substrate, while the non-chiral ones were constituted by bare p-GaAs. Although the spin-dependent ET to $MV^{+\bullet}$ was visible in both cases, the lower than expected effect on bare p-GaAs could be attributed to the presence of SS that caused partial spin relaxation, and also to the low semiconductor surface stability. Actually, both SS removal and electrode stability enhancement must be achieved to facilitate spin dependent studies in solution when using $MV^{+\bullet}$ as redox mediator, which has so far been reported as the best probe for spin-dependent studies.[15]

Previously GaAs/electrolyte interfaces have been stabilised by functionalising the semiconductor surface with self-assembled monolayers.[22–28] The surface grafting was also shown to modify the energetics and the electron transport properties of the interface.[29–32] Among the best characterised functionalisation methods is the use of aromatic rings in combination with thiol chemistry.[33–41]

Here we report the effect of biphenyl-4-thiol (B4t) functionalisation on the surface stability of p-GaAs in acetonitrile under weak illumination when using $MV^{+\bullet}$ as the redox mediator. We show that the functionalisation can remove the unwanted non-spin polarised ET processes present even in the dark, while maintaining the photo-induced ET from the CB. Also, we show that the B4t layer does not hinder the ET efficiency related to $MV^{+\bullet}$ reduction.

The B4t modified p-GaAs electrode surfaces were characterised by X-Ray Photoelectron Spectroscopy (XPS) and Atomic Force Microscopy (AFM), while their electrochemical behaviour was qualified by cyclic voltammetry (CV) and Electrochemical Impedance Spectroscopy (EIS).

2. Experimental

2.1. Materials

All sample solutions were prepared from dry acetonitrile (ACN, Acros Organics, 99.9 %, extra dry) with 0.2 M tetrabutylammonium perchlorate (TBAP, Sigma-Aldrich, ≥99.0 %) as supporting electrolyte. All samples were prepared and stored in a glove box and taken out only in a sealed glass tube prior to experiments. Methyl viologen dichloride hydrate (MV^{2+}, Sigma-Aldrich, 98%) was used as redox mediator. Biphenyl-4-thiol (B4t, Sigma-Aldrich, 97 %) was employed to functionalise the p-GaAs surface in extra dry ethanol (Acros Organics, 99.5 %).

Single crystal p-GaAs with Arsenic rich [111]B orientation (2.9×10^{17} cm^{-3} Zn-doping) was used as working electrode (WE). An ohmic contact was established to the back side by evaporating 200 nm gold after oxygen plasma etching the wafer from both sides. This contacting method has previously been found to be adequate for electrochemical experiments.[9,42,43] A copper wire was contacted to the gold layer with silver paste, and the contact was protected from the sample solution with silicone.

2.2. Methods

The general procedure for p-GaAs functionalisation with a thiol containing monolayers has been well documented.[33,38] Briefly, wafers were sonicated in acetone for 3 min and then rinsed with Milli-Q water (18.2 MOhm/cm). Then the wafers were etched in 6 M HCl for 60 s, rinsed with Milli-Q water and ethanol before dipping into a functionalisation solution (2 mM B4t in dry EtOH). The wafers were incubated at 50°C for 20 h inside a glove box after which they were sonicated for 30 s in absolute ethanol, rinsed with absolute ethanol and finally blown dry with nitrogen.

Journal Pre-proof

The non-functionalised electrodes were prepared as described above concerning the functionalised electrodes up to the point of incubation in the B4t solution. All electrodes were stored in a glove box and only taken out in an assembled and sealed test tube.

The experiments were performed in a 3 mm by 3 mm ID square glass tube. Due to the limited size of the tube, a Pt wire tip and a Pt coil were used as pseudo-reference electrode (RE) and counter electrode (CE), respectively. The potential of the Pt tip RE was compared to that of an organic Ag/Ag^+ RE, where an Ag wire was immersed into an ACN solution containing 0.2 M of TBAP and 0.01 M of $AgNO_3$. The Ag/Ag^+ RE was separated from the sample solution by a frit. All of the electrochemical data has been adjusted to the potential of the Ag/Ag^+ couple, as described in S1 (supplementary information).

A 830 nm laser diode was used as a light source, where the non-collimated light was guided to the electrode surface through a channel while protecting the electrochemical cell from the ambient light. A Gamry potentiostat (Interface 1000E) was used to record the CV and EIS data. The EIS was performed from 0.5 Hz to 100 kHz with 10 mV modulation of the electrode potential, recording 6 points per decade. Thanks to the low laser intensities used, all the EIS data were recorded under a steady state current, limited by the availability of the CB electrons.

A two compartment U-cell was used to generate $MV^{+\bullet}$ by electrolysis from MV^{2+} at a Pt electrode, where a frit separating the two sides of the cell prevented the diffusion of the counter electrode species to the sample solution. The final concentration of $MV^{+\bullet}$ was either 1 or 2 mM in 0.2 M TBAP used as supporting electrolyte. Before starting the electrolysis, MV^{2+} solutions were heated gently to promote the solubility of the mediator. The MV^{2+} was converted to $MV^{+\bullet}$ quantitatively. To ensure the complete electrolysis after depleting $[MV^{2+}]$ close to zero, small amounts of MV^0 were generated in the U-cell to convert the residual amount of MV^{2+} thanks to the comproportionation reaction described by equation 2 below. The final composition of the sample solution was checked with a 10 µm diameter Pt ultramicroelectrode (UME) to confirm that the electrolysis was complete (see S2, supplementary information).

2.3. Surface characterisation

Atomic Force Microscopy (AFM) measurements were recorded with a Park Systems model XE-100 atomic force microscope scanning a 1 µm by 1 µm surface area**.** Three samples were studied: 1) a native surface sonicated 3 min in acetone and rinsed with Milli-Q water and EtOH, 2) sonicated 3 min in acetone, rinsed with Milli-Q water, etched 60 sec in 6M HCl followed by Milli-Q and EtOH rinse, 3) as 2) but subsequently functionalised in a B4t solution followed by sonicating 30 s in EtOH and EtOH rinse. The AFM tip used was an OTESPA-R3 from Bruker with a spring constant and a resonance frequency of 26 N/m and 300 kHz, respectively.

X-Ray Photoelectron Spectroscopy (XPS) measurements were carried out using a PHI VersaProbe II scanning XPS microprobe (Physical Instruments AG, Germany). Analyses were performed using a monochromatic Al Kα X-ray source at 24.8 W power with a beam size of 100 µm. The pass energy was 20 eV yielding a full width at half maximum of 0.70 eV for the Ag 3d 5/2 peak. The spectra were corrected for C-1s (C-C) peak at 285.0 eV. The peaks were fitted with a Voigt profile.[38,44] Either a Shirley or a Tougaard type background was subtracted from the raw data, depending on the type of the background and the chemical specie under investigation. Three samples identical to those listed for AFM were studied.

Journal Pre-proof

3. Results and Discussion

3.1. Physical characterisation of the modified surfaces

3.1.1. XPS characterisation

Figures 1a and 1b present the regions of the XPS spectra corresponding to the signals of the As 3d and As $2p_{3/2}$ photoelectrons, respectively. In Figures a (i) and b (i) the non-treated (blue), HCl etched (red) and functionalised (black) surfaces are compared against each other, whereas in Figures a (ii) and b (ii) the XPS spectrum of the functionalised surface is deconvoluted for different chemical species present at the surface.

Focusing on As 3d spectra, Figure 1 (i) reveals the disappearance of a broad band situated around 44 and 45 eV for the HCl etched and functionalised surfaces. These two signals losses, attributed to As_2O_3 and As_2O_5,[44] are in agreement with the removal of the oxide layer from the GaAs surface. A characteristic feature of the HCl etched surface is a doublet for high elemental Arsenic (As^0) contents centred around 42.1 eV, whereas the functionalised surface displays a doublet for stoichiometric lattice Arsenic (As-Ga) centred around 41.4 eV.[33] In Figure a (ii) the functionalised surface shows the doublet attributable to the As-Ga as the main feature, and a residual As-O signal centred at 44 eV. A tentative assignment of Arsenic covalently bound to Sulphur (As-S) is visible at 42.8 eV, although strongly overlapped by the As-Ga.

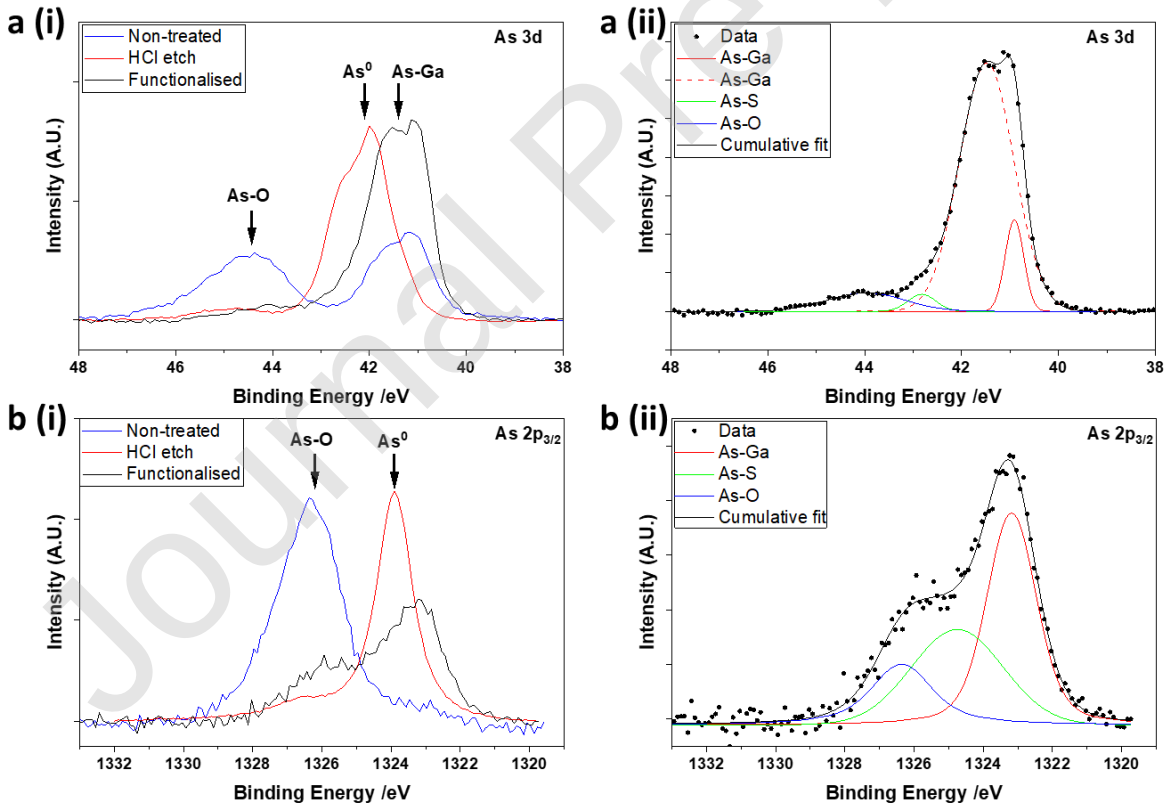

Figure 1: a (i) As 3d XPS signal for different surface treatments. a (ii) deconvolution of the 3d spectrum of the functionalised surface. b (i) As $2p_{3/2}$ signal for different surface treatments. b(ii) deconvolution of the As $2p_{3/2}$ spectrum of the functionalised surface.

Journal Pre-proof

The As $2p_{3(2}$ core-level spectra were also recorded due to their higher surface sensitivity compared to As 3d, and the results are shown in Figure 1b (i). The main feature for the non-treated surface is the strong As-O signal at 1326.2 eV, which is greatly attenuated for the HCl etched and functionalised surfaces. Likewise to the 3d spectra, the HCl etching results to the strong presence of As^0 at the surface at 1323.7 eV.[45] The deconvolution of the XPS spectrum for the functionalised surface in Figure 1b (ii) reveals a residual As-O signal at 1326.2 eV and a lattice As-Ga signal at 1323.2 eV. Most importantly, and in agreement with previous study on thiol functionalised p-GaAs 111B surface, a clear signal for As-S can be observed at 1324.8 eV, confirming the successful attachment of the B4t to the electrode surface.[38] The XPS studies also showed that the B4t modified GaAs surface was resistant to any re-oxidation within a time scale of days, even when the electrodes were left to an ambient atmosphere.

3.1.2. AFM characterisation

The surface topography was characterised by AFM on a 1 μm^2 electrode surface area. The surface morphology is shown in Figures 2a(i) to 2c(i), and the detailed surface topography in Figures 2a(ii) to 2c(ii) for native, HCl etched and B4t functionalised samples, respectively. All of the surfaces show general amorphous features, the grain size seemingly growing from native to B4t functionalised.

The untreated p-GaAs surface had a typical Root Means Square roughness (R_q) of 3.3 (±0.4) Å, in accordance with previous observations for As rich 111B surface (Fig. 2 a(i)).[37] The HCl etching prior to the functionalisation did not change the surface appreciably, providing a surface with R_q of 3.5 (±0.5) Å. The most significant change was observed for B4t functionalised surface with R_q of 8.8 (±3.3) Å.

Regarding the surface topography, HCl etching had only limited effects towards [111]B surface (2a(ii) vs 2b(ii)), indicating that the greater surface roughness observed for the B4t functionalized sample (2c(ii)) is the result of the biphenyl layer and not due to etching induced surface roughening. Together with XPS measurements, this strongly suggests that the p-GaAs surface is covered with a B4t layer, covalently bonded to the As species via As-S bonds.

Journal Pre-proof

Journal Pre-proof

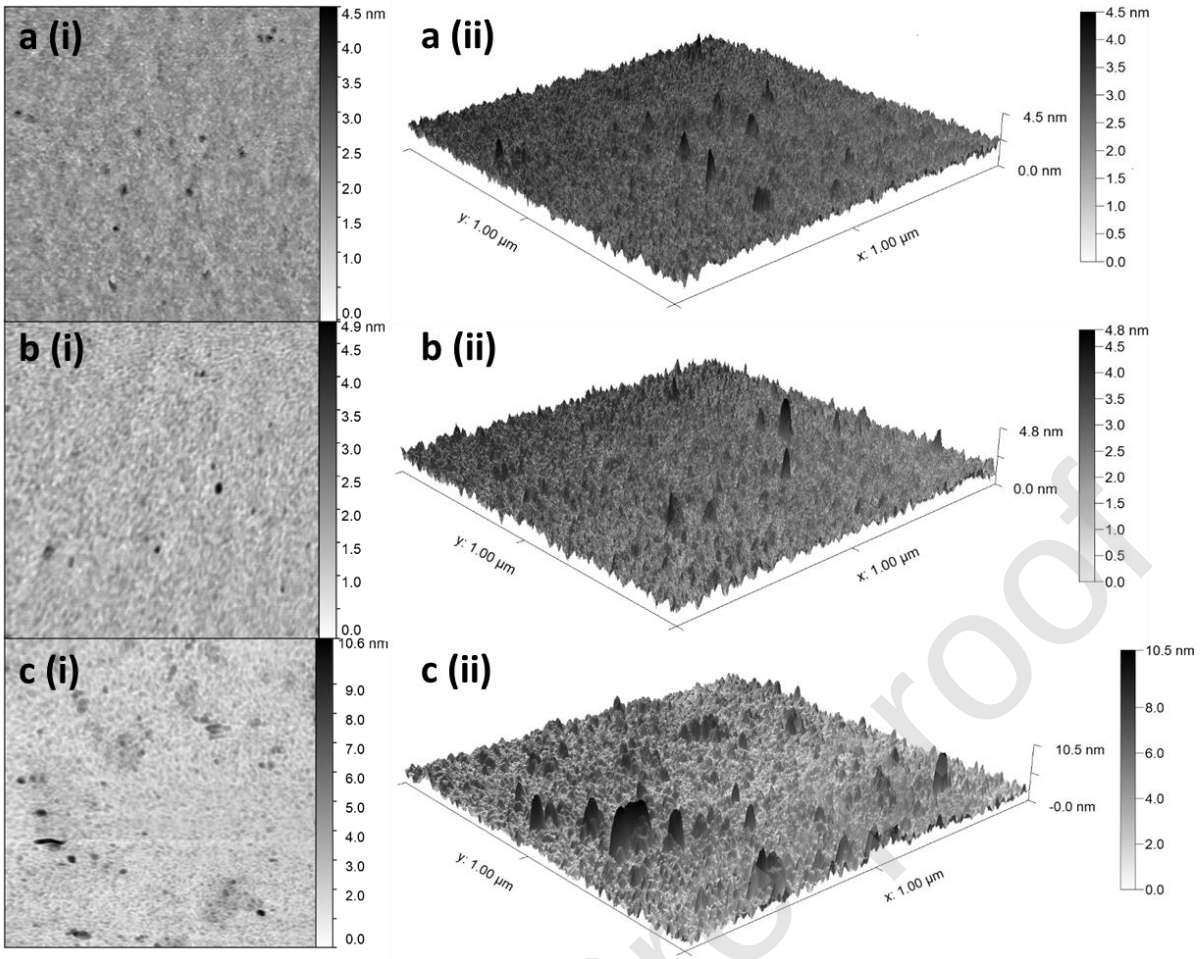

Figure 2: non-contact mode AFM images of a) untreated p-GaAs, b) HCl etched p-GaAs, c) B4t functionalised p-GaAs performed on a 1 µm² electrode surface area. Surface roughnesses of 3.3, 3.5 and 8.8 Å were measured for nontreated, HCl etched and B4t functionalised surfaces, respectively.

3.2. Electrochemical characterisation of the B4t-modified GaAs

3.2.1 General features

In acetonitrile methyl viologen di-cation MV^{2+} can go through two consecutive reduction processes, each involving one electron. The first reduction leads to a cation radical $MV^{+\bullet}$ and the second one to a neutral specie MV^0 according to equation 1:

$$MV^{2+} + e^- \rightleftarrows MV^{+\bullet} + e^- \rightleftarrows MV^0 \qquad (1)$$

Both processes are close to the reversibility with a peak to peak potential separation (ΔE_p) close to 70 mV at a 3 mm diameter Au electrode (Supplementary S1). The electrochemical process described by equation 1 is affected by a comproportionation / disproportionation reaction depicted by equation 2:

$$MV^{2+} + MV^0 \rightleftarrows 2\,MV^{+\bullet} \qquad (2)$$

The equilibrium constant for this reaction in acetonitrile has been reported to be around 1×10^7, meaning that the disproportionation of $MV^{+\bullet}$ does not occur appreciably in our conditions.[46] In addition, the dimerization of $MV^{+\bullet}$ leading to a radical spin-paired cation and/or the association of

Journal Pre-proof

$MV^{+\bullet}$ with MV^0 has been observed in aqueous solutions, but are absent in organic solvents such as propylene carbonate and acetonitrile.[47,48] Finally, $MV^{+\bullet}$ is also sensitive to O_2(g) and UV light, but working in an electrochemical cell prepared in a glove box and subsequently sealed has provided $MV^{+\bullet}$ solutions stable over time.

It should be highlighted that the electrochemical studies described below were conducted with a radical $MV^{+\bullet}$ as the bulk redox mediator obtained by the electrolysis of a solution of MV^{2+} at 1 or 2 mM (see experimental part). This is contrary to typical electrochemical studies concerning methyl viologen, where the starting species is the MV^{2+} di-cation, and highlights our need for a radical species in the bulk solution for the spin dependent charge transfer studies.[16]

3.2.2 Cyclic voltammetry

The qualitative behaviour of a p-GaAs electrode in a 1 mM $MV^{+\bullet}$ solution is shown in Figure 3a. The first redox process related to the conversion of MV^{2+} into $MV^{+\bullet}$ peaking at around – 0.9 V occurs in the dark and is almost completely independent of the light intensity (Fig. 3a black CV). This suggests a valence band (VB) and/or SS mediated charge transfer of holes, as the conduction band for a p-type semiconductor is empty in the dark.[49–51] To confirm that the observed dark process originates from VB and involves SS, electrochemical studies were performed also on a MV^{2+} solution (S3). The absence of the dark process with MV^{2+} confirmed that the source of this phenomenon is the interaction of $MV^{+\bullet}$ with the p-GaAs surface, likely generating SS energetically at or close to the formal potential of the $MV^{+\bullet/2+}$.

A strong laser illumination (260 µW) introduces the second redox process, related to the conversion of $MV^{+\bullet}$ into MV^0, peaking at around -1.2 V and arising from the transfer of the CB electrons of the semi-conductor.

Another interesting feature in Figure 3a is the shape of the oxidation peak corresponding to the $MV^{+\bullet}/MV^0$ redox couple during the backward scan which is presumably composed of two peaks. One can notice the inversion of the peak potentials for the $MV^{+\bullet}/MV^0$ redox couple, the oxidation peak being situated at a more negative potential than the reduction peak during the forward scan. This could be attributed to a VB mediated oxidation, where the energetic overlap between the VB edge or SS and the density of states of MV^0 species at the interface determines the oxidation process, not the energy of the Fermi-level which is continuously changed during the potential sweep.

Journal Pre-proof

Journal Pre-proof

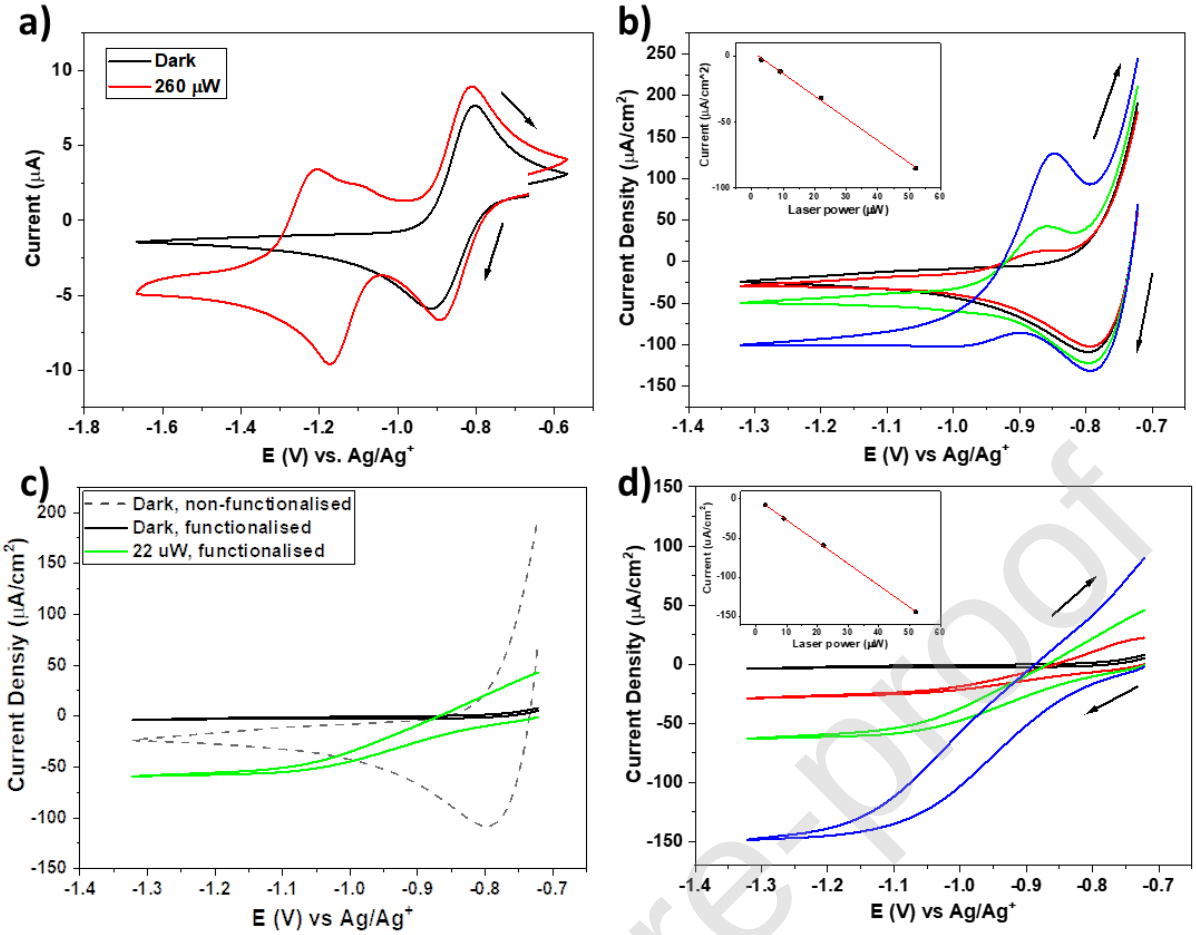

Figure 3: a) cyclic voltammograms in the dark (black) and under 260 µW laser irradiation (red) for a 1 mM $MV^{+\bullet}$ solution in dry acetonitrile with 0.2 M TBAP as supporting electrolyte. The potential window is wide enough to show both of the redox processes described in eq. 1 and their dependency on the illumination conditions. b) The quantitative behaviour for the reduction of $MV^{+\bullet}$ to MV^0 under varying laser intensities for bare p-GaAs, showing that the reduction current for the 2nd redox couple is dependent on the number of CB electrons. c) The effect of functionalising the p-GaAs with B4t monolayer compared to a non-functionalised p-GaAs. d) The quantitative behaviour of B4t functionalised electrode as a function of laser intensity. Colour legend for CVs from b to d: black = 0 µW, red = 9 µW, green = 22 µW, blue = 52 µW. All CVs were recorded at 100 mV/s.

Figure 3b shows the quantitative current response of a bare p-GaAs electrode towards low laser intensities. The dark process corresponding to the $MV^{+\bullet}/MV^{2+}$ redox couple at around -0.8 V was again present and largely independent of the laser intensity. The current that belongs to the second redox couple $MV^0/MV^{+\bullet}$ exhibited a steady state profile, and the current of this plateau increased linearly with the laser power when measured at the potential of -1.32 V (Fig. 3b inset). At low laser intensity, there were no significant changes in the plateau current while changing the CV's scan rate (S4), thus confirming that the current was limited by the availability of the CB electrons and not by the diffusion of $MV^{+\bullet}$ to the electrode surface.[13] On the return scan the anodic current peak around -0.85 V can be assigned to the oxidation of MV^0, the intensity of which was proportional to the amount of MV^0 generated during the forward scan and thus to the laser intensity.

Figure 3c shows the behaviour of a p-GaAs surface functionalised with B4t (black and green CVs), and its comparison with a non-functionalised one (dashed black line). The dark process that was observed for the non-functionalised p-GaAs has vanished completely, suggesting that the SS mediated hole transfer has been suppressed and that the surface is now stable towards $MV^{+\bullet}$. The effect of the laser

Journal Pre-proof

irradiation on the functionalised electrode is described by the green CV, which shows that the photo-generated CB electrons are still transferred to the $MV^{+\bullet}$ radicals, thus attesting that the photo induced ET was not hindered by the surface modification.

Figure 3d shows the dependency of the photo current on the laser intensity for B4t functionalised p-GaAs. As for the bare surface, the limiting photocurrent at -1.32 V still evolved linearly with the laser power (Fig. 3d inset). When compared to a non-functionalised electrode (Fig. 3b), one can observe the suppression of the dark process related to $MV^{+\bullet}/MV^{2+}$ but also the disappearance of the oxidation of MV^0 during the return scan at around -0.85 V whatever the applied laser power. The removal of this latest feature is most likely due to the suppression of the SS at the interface by the B4t layer, thus preventing any SS mediated charge transfer between VB and MV^0.

When normalising the plateau currents in Figures 3b and 3d also by the laser power incident to the electrode surface (data not shown, see [21] for the measurement method), the quantum yields were found to be 41 and 37 (±3) % for the functionalised and non-functionalised electrodes, respectively. Also, the slopes of the plateau currents *vs* the laser power plots (Figs. 3b and d insets) were found to be -1.67 and -2.77 for the non-functionalised and the functionalised electrodes, respectively, suggesting that the functionalised surface was slightly more sensitive to the laser irradiation.

Most importantly, the bi-phenyl monolayer does not seem to passivate the p-GaAs towards ET, which has been the case in aqueous solvents.[27,33,34,52] Thus, while clearly attenuating the unwanted VB/SS charge transfer, the B4t monolayer maintains the facility of the charge transfer between the p-GaAs and $MV^{+\bullet}$, as could be expected from π-electron containing biphenyl rings.[40,53–55]

Figure 4 summarises the energetics of the interface for bare (4a) and functionalised (4b) surfaces in the dark. The flat band potentials were determined by recording Mott-Schottky plots in indifferent electrolyte, and in the presence of $MV^{+\bullet}$ radical (S5) in the dark and under low light intensities. The Mott-Schottky analyses revealed that the band edges remain pinned at the electrode surface under weak illumination for both surfaces if $MV^{+\bullet}$ is present, and therefore the situation shown applies also under our experimental conditions. Based on this information the VB and the CB edges at the electrode surface could be drawn to Ag/Ag^+ scale, and compared to the formal potentials of the two redox couples of the MV ($E_1^{0\prime}$ and $E_2^{0\prime}$).

Figure 4a presents the interface in the presence of 1 mM $MV^{+\bullet}$ in the dark. The Fermi-level (E_F) pinning was observed, and the OCP always equilibrated to -0.82 V (± 5 mV), very close to the $E_1^{0\prime}$ of the $MV^{+\bullet/2+}$ couple (-0.735 V). The VB edge is situated at -0.06 V vs Ag/Ag^+, placing the CB edge to -1.48 V, 0.35 V above the $E_2^{0\prime}$ of the $MV^{0/+\bullet}$ couple, indicating a band bending of 0.67 V at the equilibrium. Based on the proposed energy diagram, it is difficult to explain the nearly reversible dark process observed in Figure 3a. The oxidation of $MV^{+\bullet}$ can readily occur through an electron transfer to the VB, but the reduction of MV^{2+} without the presence of photoelectrons remains problematic. Tentatively the SS of p-GaAs could equilibrate with the $E_1^{0\prime}$ of $MV^{+\bullet/2+}$ couple and thus facilitate an electron transfer to the MV^{2+} species. [56] Therefore we have added the SS to in the vicinity of the $E_1^{0\prime}$ to the proposed diagram in 3a, although we stress that the dark process is specific to the use of $MV^{+\bullet}$ as a starting species, and was not observed when using MV^{2+} as a bulk redox mediator (S3).

As for the observed photoreduction of the $MV^{0/+\bullet}$ couple, the CB edge is 0.35 V above the $E_2^{0\prime}$. This indicates that a wide range of reorganisation energies could bring the density of states of the oxidized species of the $MV^{0/+\bullet}$ couple to overlap with the CB edge, thus facilitating the second reduction process. When considering the oxidation processes for both couples during the return scan (Fig. 3a), we assume a VB process, as the densities of states of the MV^0 do not overlap with the CB edge. This

notion is supported by previous work conducted with n-GaAs in water/EtOH (1:1) mixture in the dark, where during a forward scan two reduction peaks were observed for MV^{2+}, whereas in the return scan no oxidative processes were observed, as the holes were absent from the VB.[57] This is contrary to the observations made in aqueous solutions at pH 2, where the oxidation of MV^0 has been observed to occur via an electron injection to the CB of n-GaAs.[58]

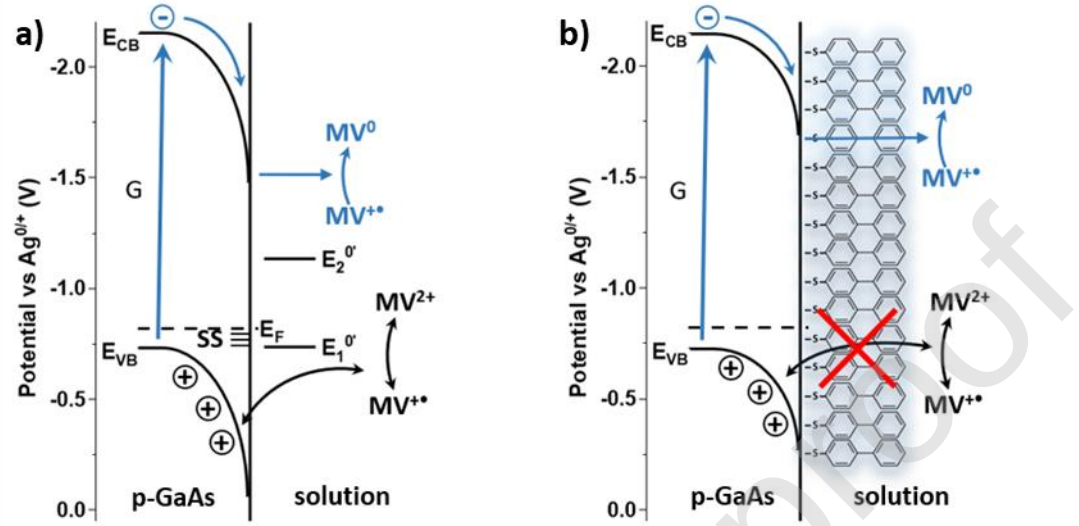

Figure 4: Energetics of the interface in the presence of 1 mM $MV^{+\bullet}$. a) Charge transfer processes for bare p-GaAs electrode. Black arrows: In the dark the CB is empty and the observed redox process for the $MV^{+\bullet}/MV^{2+}$ couple is SS mediated. Blue arrows: Laser illumination (G) generates photoelectrons to CB, which can either participate to the reduction of $MV^{+\bullet}$ to MV^0, or relax back to the VB via the SS where they recombine with holes. b) Charge transfer for functionalised p-GaAs. The B4t layer prevents the interaction between $MV^{+\bullet}$ and the electrode surface, thus removing the dark process. Laser irradiation still generates photoelectrons which reduce $MV^{+\bullet}$ to MV^0 with unhindered efficiency.

For the functionalised surface in Figure 4b the interfacial processes are simplified. The VB edge is now situated at -0.27 V vs Ag/Ag^+, placing the CB edge to -1.69 V. Exactly the same Fermi-level pinning was observed as for the bare surface however (-0.82 V), suggesting a band bending of 0.46 V at the equilibrium. As shown in Figure 3, the functionalisation of the p-GaAs surface with a B4t monolayer removes the dark process occurring from the VB completely, and only the reduction initiated from the CB by photoelectrons takes place. This is clearly attributable to the effect of the B4t monolayer blocking the interaction between the $MV^{+\bullet}$ and the electrode surface. Thus, we have not drawn any SS contribution to the interface, as the EIS data presented below effectively suggested their absence from the interface.

Journal Pre-proof

Journal Pre-proof

3.2.3. Electrochemical Impedance Spectroscopy

EIS was used to characterise the B4t-modified GaAs electrodes. The equivalent circuit used to fit the impedance data is presented in Figure 5a. Similar circuit has been suggested before for 4,4'-thio-bis-benzene-thiolate and biphenyl 4,4' –dithiol functionalised p-GaAs in H_2SO_4 solutions,[37,38] but in our case the SS and adsorption related components were removed, as their incorporation did not result to further increase in the fit quality. In addition to the solution resistance (R_{soln}), the equivalent circuit comprises two sub-circuits. The first sub-circuit is made of a parallel combination of a space charge layer capacitance (C_{SC}) with a charge transfer resistance (R_{CT}) and Warburg impedance (W). The second sub-circuit, in series with the first sub-circuit, is constituted by a monolayer capacitance (C_{B4t}) and resistance (R_{B4t}).

To improve the fit, constant phase elements (CPE) were employed instead of ideal capacitors to model any inhomogeneities of the interface. The impedance of a CPE can be defined as $Z_{CPE} = Y_0(j\omega)^{-\alpha}$ where α is the frequency component, 0 indicating a pure resistance and 1 pure capacitance.[35,59] It was also necessary to introduce a Warburg element (W) to fit the spectra at low frequencies, most likely due to the diffusion of ions within the B4t [41,60] which could indicate the existence of pinholes within the layer, or some π-π interactions between $MV^{+\bullet}$ and the biphenyl layer. The inclusion of the Warburg element clearly acts as an approximation, as this element is generally used to represent a linear diffusion across a semi-infinite space.[60]

Figure 5b shows the EIS spectra of the functionalised electrode stepped to a potential of -1.32 V (i.e. at the limiting current, see Fig. 3d) in the dark and when illuminated with a laser at 9 and 22 µW powers for a 2 mM $MV^{+\bullet}$ solution. The solid lines are the corresponding EIS fits utilising the circuit depicted in Figure 5a.

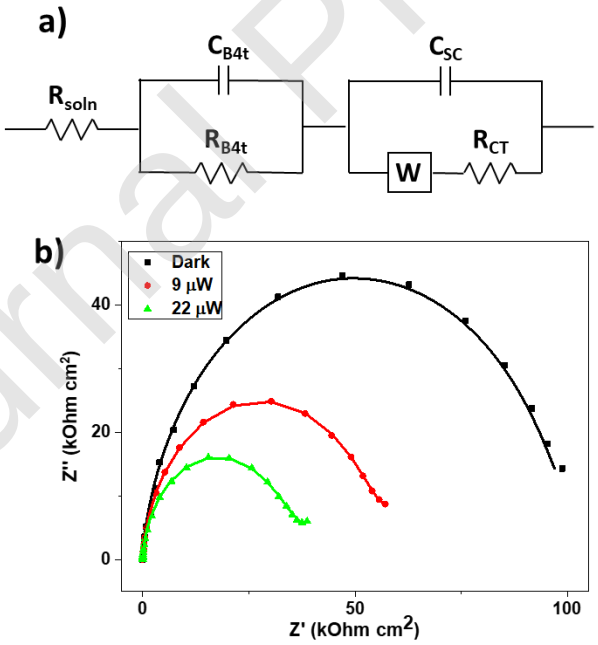

Figure 5a: Equivalent circuit for fitting the EIS data, showing a parallel combination of the B4t capacitance (C_{B4t}) and resistance (R_{B4t}) in series with a parallel combination of the space charge capacitance (C_{SC}) and the charge transfer resistance (R_{CT}). b) EIS response for the biphenyl functionalised electrode at the potential of -1.32 V (i.e. the limiting current, see Fig. 3d)) immersed in a 2 mM $MV^{+\bullet}$ solution in dry acetonitrile with 0.2 M TBAP as supporting electrolyte.

Journal Pre-proof

Most importantly, the possibility to fit the EIS data without incorporating the SS effects confirms that their influence is negligible for the B4t modified electrodes. This has already been observed for functionalised GaAs, namely that the SS capacitance (C_{SS}) is not detectable in EIS spectra if C_{SS} / C_{SC} < 0.1,[35,52] and the same assumption was used also here to simplify the fitting and analysis of the EIS data.[61,62] The missing influence of the SS in the EIS data correlates with the absence of the oxidative peaks in the return scans for the CVs displayed in Figure 3d. This finding further confirms that the oxidation of MV^0 on non-functionalised electrodes involves the SS, a process which is clearly hindered for the functionalised surfaces.

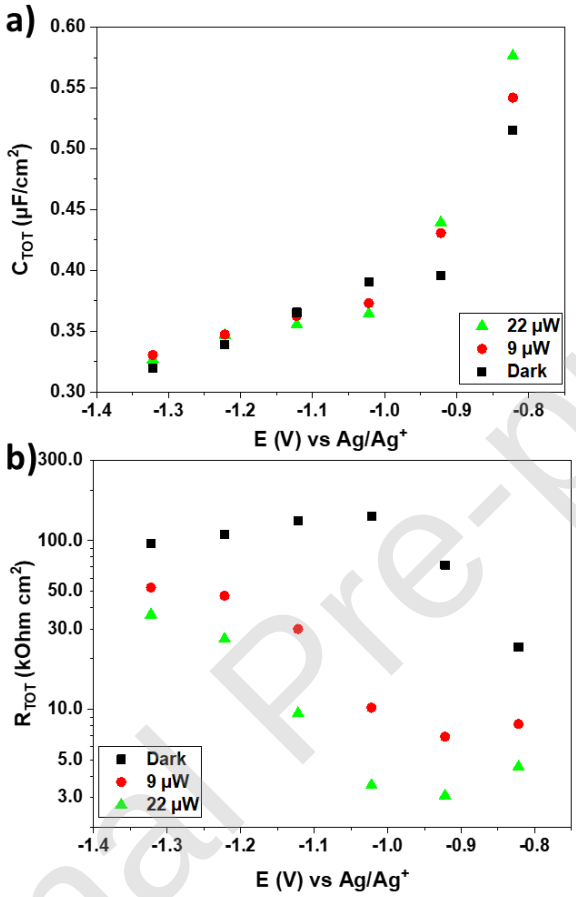

Figure 6: Results for the EIS measurements for 2 mM $MV^{+\bullet}$ solution in dry acetonitrile with 0.2 M TBAP as supporting electrolyte at B4t functionalised p-GaAs. *a) The series capacitance (C_{TOT}) of the interface. b) the combined series resistance R(TOT) of the interface.*

Figure 6a shows the capacitance of the entire interface (C_{TOT}) as a function of the applied potential and the laser power. This equivalent capacitance, already used to model modified GaAS electrodes,[33–35] is expressed as:

$$C_{TOT} = \frac{C_{B4t} C_{SC}}{C_{B4t} + C_{SC}} \qquad (3)$$

As the frequency ranges for the C_{B4t} and the C_{SC} overlapped during an EIS measurement, it was difficult to distinguish between the different capacitance contributions. Indeed, it was possible to fit the EIS

Journal Pre-proof

data recorded at -1.32 V with a simple Randles circuit without losing any quality of the fit while obtaining results within a couple of % points from those with Eq. 3. We have attempted to deconvolute the EIS data to individual C_{B4t}, C_{SC}, R_{B4t} and R_{CT} values in S6.

The C_{TOT} value for the B4t coated p-GaAs has been measured before to be 0.45 μF/cm^2.[34] Although performed in aqueous solvent, this result is similar order of magnitude than our results in Fig. 6a, which shows the decreasing C_{TOT} with increasing bias. The α value of the B4t CPE was above 0.95 for all the measurements, indicating that the B4t SAM behaved almost as a pure capacitance.

Figure 6b shows the total resistance R_{TOT} of the interface as a function of the applied potential and the light intensity. As observed, R_{TOT} is strongly influenced by the applied potential and the laser intensity, the dominant component being the R_{CT} rather than R_{B4t} (S6). The increasing laser intensity diminishes the overall resistance, as the current increases and the rate of Faradaic reduction increases. The fact that the R_{B4t} contributes only slightly towards the overall charge transfer resistance is promising for spin dependent experiments, as the monolayer is not expected to introduce significant hindrance towards the rate of ET and thus towards unwanted relaxation of the spin polarisation.

As a comparison, systematic EIS studies performed on non-functionalised p-GaAs in $MV^{+\bullet}$ solutions turned out to be unsuccessful, partly due to the instability of the p-GaAs in presence of the radical species, and partly due to the complicated dark process that could not be satisfactorily fitted to any feasible equivalent circuit.

4. Conclusions

Functionalising p-GaAs with B4t monolayer was shown to stabilise the semiconductor surface against $MV^{+\bullet}$ radical, removing the SS mediated unwanted $MV^{+\bullet}/MV^{2+}$ process that was observed even in the dark on bare p-GaAs. The EIS analyses of the functionalised surface revealed that a simple space charge-monolayer model fitted the data adequately, and the addition of more fitting parameters was not needed. This suggests that the influence of the SS at the interface was attenuated to a lower level, *i.e.* not detectable by electrochemical methods.

This situation is ideal for future studies on spin dependent processes at p-GaAs under optical excitation, as radicals required in the sample solution will not destabilise the electrode, and the absence of SS at the interface should lead to lesser degree of SS mediated relaxation of electrons from the CB to VB.

The passivation of the electrode surface against unwanted processes did not lead to a lower Faradaic yield, displaying the ability of the biphenyl monolayer to facilitate the electron transfer from the CB of the p-GaAs to the radical in the solution. This is contrary to previous studies in aqueous solution, where up to 50 fold increase in the interfacial resistance after functionalisation has been observed.[33,34] However, the stability of the interface was far from that observed in aqueous solutions (up to 22h) most likely due to some π-π interactions between $MV^{+\bullet}$ and the biphenyl layer, providing a stable photo-response up to a couple of hours only, depending on the magnitude of the photocurrents generated.

Author Statement

The authors declare no competing financial or personal interests.

Journal Pre-proof

Declaration of interest

The authors declare no competing financial or personal interests.

Acknowledgments

We gratefully acknowledge funding by the Swiss National Science Foundation (Grants 200021_160182 and 200020_169515) and Rothschild Caesarea Foundation, Caesarea Business Park, 38900 Caesarea, Israel (Grant 6115).

References

(1) Campesato, R.; Tukiainen, A.; Aho, A.; Gori, G.; Isoaho, R.; Greco, E.; Guina, M. 31% European InGaP/GaAs/InGaAs Solar Cells for Space Application. *E3S Web Conf.* **2017**, *16*, 03003. https://doi.org/10.1051/e3sconf/20171603003.

(2) Hirota, K.; Tryk, D. A.; Yamamoto, T.; Hashimoto, K.; Okawa, M.; Fujishima, A. Photoelectrochemical Reduction of CO2 in a High-Pressure CO2 + Methanol Medium at p-Type Semiconductor Electrodes. *J. Phys. Chem. B* **1998**, *102* (49), 9834–9843. https://doi.org/10.1021/jp9822945.

(3) Kaneco, S.; Katsumata, H.; Suzuki, T.; Ohta, K. Photoelectrochemical Reduction of Carbon Dioxide at P-Type Gallium Arsenide and p-Type Indium Phosphide Electrodes in Methanol. *Chem. Eng. J.* **2006**, *116* (3), 227–231. https://doi.org/10.1016/j.cej.2005.12.014.

(4) Leest, R. H. van; Mulder, P.; Gruginskie, N.; Laar, S. C. W. van; Bauhuis, G. J.; Cheun, H.; Lee, H.; Yoon, W.; Heijden, R. van der; Bongers, E.; et al. Temperature-Induced Degradation of Thin-Film III-V Solar Cells for Space Applications. *IEEE J. Photovoltaics* **2017**, *7* (2), 702–708. https://doi.org/10.1109/JPHOTOV.2016.2642642.

(5) Petit, J.-P.; Chartier, P.; Beley, M.; Deville, J.-P. Molecular Catalysts in Photoelectrochemical Cells. *J. Electroanal. Chem. Interfacial Electrochem.* **1989**, *269* (2), 267–281. https://doi.org/10.1016/0022-0728(89)85137-X.

(6) Sears, W. M.; Morrison, S. R. Carbon Dioxide Reduction on Gallium Arsenide Electrodes. *J. Phys. Chem.* **1985**, *89* (15), 3295–3298. https://doi.org/10.1021/j100261a026.

(7) Simon, J.; Schulte, K. L.; Jain, N.; Johnston, S.; Young, M.; Young, M. R.; Young, D. L.; Ptak, A. J. Upright and Inverted Single-Junction GaAs Solar Cells Grown by Hydride Vapor Phase Epitaxy. *IEEE J. Photovoltaics* **2017**, *7* (1), 157–161. https://doi.org/10.1109/JPHOTOV.2016.2614122.

(8) Bard, A. J.; Bocarsly, A. B.; Fan, F. R. F.; Walton, E. G.; Wrighton, M. S. The Concept of Fermi Level Pinning at Semiconductor/Liquid Junctions. Consequences for Energy Conversion Efficiency and Selection of Useful Solution Redox Couples in Solar Devices. *J. Am. Chem. Soc.* **1980**, *102* (11), 3671–3677. https://doi.org/10.1021/ja00531a001.

(9) Fan, F. R. F.; Bard, A. J. Semiconductor Electrodes. 24. Behavior of Photoelectrochemical Cells Based on p-Type Gallium Arsenide in Aqueous Solutions. *J. Am. Chem. Soc.* **1980**, *102* (11), 3677–3683. https://doi.org/10.1021/ja00531a002.

(10) Kelly, J. J.; Minks, B. P.; Verhaegh, N. A. M.; Stumper, J.; Peter, L. M. Photocurrent Multiplication at P-Type Semiconductor Electrodes. *Electrochim. Acta* **1992**, *37* (5), 909–918. https://doi.org/10.1016/0013-4686(92)85042-J.

Journal Pre-proof

(11) Kohl, P. A.; Bard, A. J. Semiconductor Electrodes: XVI . The Characterization and Photoelectrochemical Behavior of N- and p-GaAs Electrodes in Acetonitrile Solutions. *J. Electrochem. Soc.* **1979**, *126* (1), 59–67. https://doi.org/10.1149/1.2128989.

(12) Kohl, P. A.; Bard, A. J. Semiconductor Electrodes: XVIII . Liquid Junction Photovoltaic Cells Based on Electrodes and Acetonitrile Solutions. *J. Electrochem. Soc.* **1979**, *126* (4), 603–608. https://doi.org/10.1149/1.2129094.

(13) Reichman, B.; Ren F. Fan, F.; J. Bard, A. Semiconductor Electrodes 25: The p-GaAs/Heptyl Viologen System. Photoelectrochemical Cells and Photoelectrochromic Displays. *J. Electrochem. Soc.* **1980**, *127* (2), 333–338. https://doi.org/10.1149/1.2129666.

(14) Modestov, A. D.; Kazarinov, V. E. Electrochemical Reduction of 2,6-Diphenylpyrylium Cations by Spin-Polarized Electrons on p-GaAs Photocathodes. *J. Electroanal. Chem.* **1993**, *346* (1–2), 353–366. https://doi.org/10.1016/0022-0728(93)85024-B.

(15) Chazalviel, J. -N. Spin-dependent Electrochemical Kinetics at a Semiconducting Photocathode. *J. Chem. Phys.* **1985**, *83* (1), 149–156. https://doi.org/10.1063/1.449797.

(16) Blumenschein, F.; Tamski, M.; Roussel, C.; Smolinsky, E. Z. B.; Tassinari, F.; Naaman, R.; Ansermet, J.-P. Spin-Dependent Charge Transfer at Chiral Electrodes Probed by Magnetic Resonance. *Phys. Chem. Chem. Phys.* **2020**, *22* (3), 997–1002. https://doi.org/10.1039/C9CP04681J.

(17) Vanmaekelbergh, D. Direct and Surface State Mediated Electron Transfer at Semiconductor/Electrolyte Junctions—II. A Comparison of the Interfacial Admittance. *Electrochim. Acta* **1997**, *42* (7), 1135–1141. https://doi.org/10.1016/S0013-4686(96)00266-6.

(18) Vanmaekelbergh, D. Direct and Surface State Mediated Electron Transfer at Semiconductor/Electrolyte Junctions—I. A Comparison of Steady-State Results. *Electrochim. Acta* **1997**, *42* (7), 1121–1134. https://doi.org/10.1016/S0013-4686(96)00265-4.

(19) Gerischer, H. Electron-Transfer Kinetics of Redox Reactions at the Semiconductor/Electrolyte Contact. A New Approach. *J. Phys. Chem.* **1991**, *95* (3), 1356–1359. https://doi.org/10.1021/j100156a060.

(20) Gomes, W. P.; Vanmaekelbergh, D. Impedance Spectroscopy at Semiconductor Electrodes: Review and Recent Developments. *Electrochim. Acta* **1996**, *41* (7–8), 967–973. https://doi.org/10.1016/0013-4686(95)00427-0.

(21) Tamski, M.; Blumenschein, F.; Roussel, C.; Ansermet, J.-P. Probing Charge Transfer Processes at P-GaAs Electrodes under Weak Optical Excitation. *J. Photochem. Photobiol. A Chem.* **2019**, *382*, 111894. https://doi.org/10.1016/j.jphotochem.2019.111894.

(22) Cho, Y.; Ivanisevic, A. Mapping the Interaction Forces between TAR RNA and TAT Peptides on GaAs Surfaces Using Chemical Force Microscopy. *Langmuir* **2006**, *22* (4), 1768–1774. https://doi.org/10.1021/la052729x.

(23) Kaindl, T.; Adlkofer, K.; Morita, T.; Umemura, J.; Konovalov, O.; Kimura, S.; Tanaka, M. Modulation of Band Bending of Gallium Arsenide with Oriented Helical Peptide Monolayers. *J. Phys. Chem. C* **2010**, *114* (51), 22677–22683. https://doi.org/10.1021/jp110133t.

(24) Traub, M. C.; Biteen, J. S.; Michalak, D. J.; Webb, L. J.; Brunschwig, B. S.; Lewis, N. S. Phosphine Functionalization of GaAs(111)A Surfaces. *J. Phys. Chem. C* **2008**, *112* (47), 18467–18473. https://doi.org/10.1021/jp803992h.

(25) Vidoni, O.; Neumeier, S.; Bardou, N.; Pelouard, J.-L.; Schmid, G. Self-Assembly of Gold

Journal Pre-proof

Nanoclusters on Molecularly Modified GaAs. *J. Clust. Sci.* **2003**, *14* (3), 325–336. https://doi.org/10.1023/B:JOCL.0000005067.63818.39.

(26) Wu, L.; Camacho-Alanis, F.; Castaneda, H.; Zangari, G.; Swami, N. Electrochemical Impedance Spectroscopy of Carboxylic-Acid Terminal Alkanethiol Self Assembled Monolayers on GaAs Substrates. *Electrochim. Acta* **2010**, *55* (28), 8758–8765. https://doi.org/https://doi.org/10.1016/j.electacta.2010.08.001.

(27) Adlkofer, K.; Tanaka, M.; Hillebrandt, H.; Wiegand, G.; Sackmann, E.; Bolom, T.; Deutschmann, R.; Abstreiter, G. Electrochemical Passivation of Gallium Arsenide Surface with Organic Self-Assembled Monolayers in Aqueous Electrolytes. *Appl. Phys. Lett.* **2000**, *76* (22), 3313–3315. https://doi.org/10.1063/1.126636.

(28) Luber, S. M.; Adlkofer, K.; Rant, U.; Ulman, A.; Gölzhäuser, A.; Grunze, M.; Schuh, D.; Tanaka, M.; Tornow, M.; Abstreiter, G. Liquid Phase Sensors Based on Chemically Functionalized GaAs/AlGaAs Heterostructures. *Phys. E Low-dimensional Syst. Nanostructures* **2004**, *21* (2–4), 1111–1115. https://doi.org/10.1016/j.physe.2003.11.189.

(29) Gartsman, K.; Cahen, D.; Kadyshevitch, A.; Libman, J.; Moav, T.; Naaman, R.; Shanzer, A.; Umansky, V.; Vilan, A. Molecular Control of a GaAs Transistor. *Chem. Phys. Lett.* **1998**, *283* (5), 301–306. https://doi.org/https://doi.org/10.1016/S0009-2614(97)01387-0.

(30) Seker, F.; Meeker, K.; Kuech, T. F.; Ellis, A. B. Surface Chemistry of Prototypical Bulk II−VI and III−V Semiconductors and Implications for Chemical Sensing. *Chem. Rev.* **2000**, *100* (7), 2505–2536. https://doi.org/10.1021/cr980093r.

(31) Vilan, A.; Cahen, D. How Organic Molecules Can Control Electronic Devices. *Trends Biotechnol.* **2002**, *20* (1), 22–29. https://doi.org/10.1016/S0167-7799(01)01839-X.

(32) Wu, D. G.; Cahen, D.; Graf, P.; Naaman, R.; Nitzan, A.; Shvarts, D. Direct Detection of Low-Concentration NO in Physiological Solutions by a New GaAs-Based Sensor. *Chemistry (Easton).* **2001**, *7* (8), 1743–1749. https://doi.org/10.1002/1521-3765(20010417)7:8<1743::AID-CHEM17430>3.0.CO;2-X.

(33) Adlkofer, K.; Shaporenko, A.; Zharnikov, M.; Grunze, M.; Ulman, A.; Tanaka, M. Chemical Engineering of Gallium Arsenide Surfaces with 4‘-Methyl-4-Mercaptobiphenyl and 4‘-Hydroxy-4-Mercaptobiphenyl Monolayers. *J. Phys. Chem. B* **2003**, *107* (42), 11737–11741. https://doi.org/10.1021/jp0356719.

(34) Adlkofer, K.; Eck, W.; Grunze, M.; Tanaka, M. Surface Engineering of Gallium Arsenide with 4-Mercaptobiphenyl Monolayers. *J. Phys. Chem. B* **2003**, *107* (2), 587–591. https://doi.org/10.1021/jp0267813.

(35) Gassull, D.; Luber, S. M.; Ulman, A.; Grunze, M.; Tornow, M.; Abstreiter, G.; Tanaka, M. PH Sensitivity of Gallium Arsenide (GaAs) Electrodes Functionalized with Methyl−mercaptobiphenyl Monolayers. *J. Phys. Chem. C* **2007**, *111* (33), 12414–12419. https://doi.org/10.1021/jp072952y.

(36) Lu, H.; Zharnikov, M. Structure-Building Forces in Biphenyl-Substituted Alkanethiolate Self-Assembled Monolayers on GaAs(001): The Effect of the Bending Potential. *J. Phys. Chem. C* **2015**, *119* (49), 27401–27409. https://doi.org/10.1021/acs.jpcc.5b07067.

(37) Preda, L.; Anastasescu, M.; Dobrescu, G.; Negrila, C.; Lazarescu, V. Role of the Dithiolate Backbone on the Passivation of P-GaAs(111)B Surface. *J. Electroanal. Chem.* **2016**, *771* (Supplement C), 56–63. https://doi.org/https://doi.org/10.1016/j.jelechem.2016.03.046.

(38) Preda, L.; Negrila, C.; Lazarescu, M. F.; Enache, M.; Anastasescu, M.; Toader, A. M.; Ionescu,

Journal Pre-proof

S.; Lazarescu, V. Ga and As Competition for Thiolate Formation at P-GaAs(1 1 1) Surfaces. *Electrochim. Acta* **2013**, *104*, 1–11. https://doi.org/https://doi.org/10.1016/j.electacta.2013.04.077.

(39) Shaporenko, A.; Adlkofer, K.; Johansson, L. S. O.; Ulman, A.; Grunze, M.; Tanaka, M.; Zharnikov, M. Spectroscopic Characterization of 4'-Substituted Aromatic Self-Assembled Monolayers on GaAs(100) Surface. *J. Phys. Chem. B* **2004**, *108* (46), 17964–17972. https://doi.org/10.1021/jp040474a.

(40) Yamada, F.; Shirasaka, T.; Fukui, K.; Kamiya, I. Surface State Control of III–V Semiconductors Using Molecular Modification. *Phys. E Low-dimensional Syst. Nanostructures* **2010**, *42* (10), 2841–2845. https://doi.org/10.1016/j.physe.2010.01.018.

(41) Gassull, D.; Ulman, A.; Grunze, M.; Tanaka, M. Electrochemical Sensing of Membrane Potential and Enzyme Function Using Gallium Arsenide Electrodes Functionalized with Supported Membranes. *J. Phys. Chem. B* **2008**, *112* (18), 5736–5741. https://doi.org/10.1021/jp711068b.

(42) Laflère, W. .; Van Meirhaeghe, R. .; Cardon, F.; Gomes, W. . On the Frequency-Dependence of the Impedance of n- and p-Type Gallium Arsenide Electrodes. *Surf. Sci.* **1976**, *59* (2), 401–412. https://doi.org/10.1016/0039-6028(76)90025-X.

(43) Laflere, W. H.; Cardon, F.; Gomes, W. P. On the Differential Capacitance of the N- and p-Type Gallium Arsenide Electrode. *Surf. Sci.* **1974**, *44* (2), 541–552. https://doi.org/10.1016/0039-6028(74)90136-8.

(44) Traub, M. C.; Biteen, J. S.; Michalak, D. J.; Webb, L. J.; Brunschwig, B. S.; Lewis, N. S. High-Resolution X-Ray Photoelectron Spectroscopy of Chlorine-Terminated GaAs(111)A Surfaces. *J. Phys. Chem. B* **2006**, *110* (32), 15641–15644. https://doi.org/10.1021/jp061623n.

(45) Garner, L. E.; Steirer, K. X.; Young, J. L.; Anderson, N. C.; Miller, E. M.; Tinkham, J. S.; Deutsch, T. G.; Sellinger, A.; Turner, J. A.; Neale, N. R. Covalent Surface Modification of Gallium Arsenide Photocathodes for Water Splitting in Highly Acidic Electrolyte. *ChemSusChem* **2017**, *10* (4), 767–773. https://doi.org/10.1002/cssc.201601408.

(46) Bird, C. L.; Kuhn, A. T. Electrochemistry of the Viologens. *Chem. Soc. Rev.* **1981**, *10* (1), 49. https://doi.org/10.1039/cs9811000049.

(47) Kosower, E. M.; Cotter, J. L. Stable Free Radicals. II. The Reduction of 1-Methyl-4-Cyanopyridinium Ion to Methylviologen Cation Radical. *J. Am. Chem. Soc.* **1964**, *86* (24), 5524–5527. https://doi.org/10.1021/ja01078a026.

(48) van Dam, H. T.; Ponjeé, J. J. Electrochemically Generated Colored Films of Insoluble Viologen Radical Compounds. *J. Electrochem. Soc.* **1974**, *121* (12), 1555–1558.

(49) Decker, F.; Pettinger, P.; Gerischer, H. Hole Injection and Electroluminescence of N-GaAs in the Presence of Aqueous Redox Electrolytes. *J. Electrochem. Soc.* **1983**, *130* (6), 1335. https://doi.org/10.1149/1.2119948.

(50) Meissner, D.; Memming, R. Analysis of Current—Potential Characteristics of n- and p-Type Semiconductor Electrodes. *Electrochim. Acta* **1992**, *37* (5), 799–809. https://doi.org/https://doi.org/10.1016/0013-4686(92)85033-H.

(51) Van Den Meerakker, J. E. A. M. The Electrochemistry of Alkaline K3Cr(CN)6 Solutions at p-GaAs. *J. Electroanal. Chem. Interfacial Electrochem.* **1988**, *243* (1), 161–169. https://doi.org/https://doi.org/10.1016/0022-0728(88)85036-8.

Journal Pre-proof

(52) Adlkofer, K.; Tanaka, M. Stable Surface Coating of Gallium Arsenide with Octadecylthiol Monolayers. *Langmuir* **2001**, *17* (14), 4267–4273. https://doi.org/10.1021/la001507q.

(53) Kockmann, D.; Poelsema, B.; Zandvliet, H. J. W. Transport through a Single Octanethiol Molecule. *Nano Lett.* **2009**, *9* (3), 1147–1151. https://doi.org/10.1021/nl803767c.

(54) Xiao; Xu; Tao, N. J. Measurement of Single Molecule Conductance: Benzenedithiol and Benzenedimethanethiol. *Nano Lett.* **2004**, *4* (2), 267–271. https://doi.org/10.1021/nl035000m.

(55) Fletcher, S. The Theory of Electron Transfer. *J. Solid State Electrochem.* **2010**, *14* (5), 705–739. https://doi.org/10.1007/s10008-009-0994-z.

(56) Ba, B.; Fotouhi, B.; Gabouze, N.; Gorochov, O.; Cachet, H. Dependence of the Flat-Band Potential of n-Type GaAs on the Redox Potential in Methanol and Acetonitrile. *J. Electroanal. Chem.* **1992**, *334* (1), 263–277. https://doi.org/https://doi.org/10.1016/0022-0728(92)80577-Q.

(57) Hens, Z.; Gomes, W. P. Electrochemical Impedance Spectroscopy at Semiconductor Electrodes: The Recombination Resistance Revisited. *J. Electroanal. Chem.* **1997**, *437* (1), 77–83. https://doi.org/http://dx.doi.org/10.1016/S0022-0728(97)00092-2.

(58) Schoenmakers, G. H.; Waagenaar, R.; Kelly, J. J. Methylviologen Redox Reactions at Semiconductor Single Crystal Electrodes. *Berichte der Bunsengesellschaft für Phys. Chemie* **1996**, *100* (7), 1169–1175. https://doi.org/10.1002/bbpc.19961000712.

(59) Lee, F.-Y.; Yang, K.-Y.; Wang, Y.-C.; Li, C.-H.; Lee, T. R.; Lee, T.-C. Electrochemical Properties of an AgInS2 Photoanode Prepared Using Ultrasonic-Assisted Chemical Bath Deposition. *RSC Adv.* **2014**, *4* (66), 35215–35223. https://doi.org/10.1039/c4ra01728e.

(60) Hillebrandt, H.; Tanaka, M. Electrochemical Characterization of Self-Assembled Alkylsiloxane Monolayers on Indium−Tin Oxide (ITO) Semiconductor Electrodes. *J. Phys. Chem. B* **2001**, *105* (19), 4270–4276. https://doi.org/10.1021/jp004062n.

(61) Horowitz, G.; Allongue, P.; Cachet, H. Quantitative Comparison of Fermi Level Pinning at GaAs / Metal and GaAs / Liquid Junctions. *J. Electrochem. Soc.* **1984**, *131* (11), 2563–2569.

(62) Allongue, P.; Cachet, H. Band-Edge Shift and Surface Charges at Illuminated N-GaAs/Aqueous Electrolyte Junctions: Surface-State Analysis and Simulation of Their Occupation Rate. *J. Electrochem. Soc.* **1985**, *132* (1), 45–52. https://doi.org/10.1149/1.2113788.

(63) Kelly, J. J. The Influence of Surface Recombination and Trapping on the Cathodic Photocurrent at P-Type III-V Electrodes. *J. Electrochem. Soc.* **1982**, *129* (4), 730. https://doi.org/10.1149/1.2123961.

(64) Gomes, W. P.; Cardon, F. Electron Energy Levels in Semiconductor Electrochemistry. *Prog. Surf. Sci.* **1982**, *12* (2), 155–215. https://doi.org/10.1016/0079-6816(82)90002-8.

(65) Sabatani, E.; Cohen-Boulakia, J.; Bruening, M.; Rubinstein, I. Thioaromatic Monolayers on Gold: A New Family of Self-Assembling Monolayers. *Langmuir* **1993**, *9* (11), 2974–2981. https://doi.org/10.1021/la00035a040.